



A toxicogenomic approach to assess kidney injury induced by mercuric chloride in rats



Patric Schyman^{a,b,1,*}, Richard L. Printz^{c,1}, Mohamed Diwan M. AbdulHameed^{a,b},
Shanea K. Estes^c, Chiyo Shiota^c, Masakazu Shiota^{c,**}, Anders Wallqvist^a

^a DoD Biotechnology High Performance Computing Software Applications Institute, Telemedicine and Advanced Technology Research Center, U.S. Army Medical Research and Development Command, Fort Detrick, MD, USA

^b The Henry M. Jackson Foundation for the Advancement of Military Medicine Inc., Bethesda, MD, USA

^c Department of Molecular Physiology and Biophysics, Vanderbilt University School of Medicine, Nashville, TN, USA

ARTICLE INFO

Keywords:

Predictive toxicology
RNA-seq
Mercuric chloride
Toxicogenomics
Nephrotoxicity
Necrosis

ABSTRACT

Kidney injury caused by disease, trauma, environmental exposures, or drugs may result in decreased renal function, chronic kidney disease, or acute kidney failure. Diagnosis of kidney injury using serum creatinine levels, a common clinical test, only identifies renal dysfunction after the kidneys have undergone severe damage. Other indicators sensitive to kidney injury, such as the level of urine kidney injury molecule-1 (KIM-1), lack the ability to differentiate between injury phenotypes. To address early detection as well as detailed categorization of kidney-injury phenotypes in preclinical animal or cellular studies, we previously identified eight sets (modules) of co-expressed genes uniquely associated with kidney histopathology. Here, we used mercuric chloride (HgCl₂)—a model nephrotoxicant—to chemically induce kidney injuries as monitored by KIM-1 levels in Sprague Dawley rats at two doses (0.25 or 0.50 mg/kg) and two exposure lengths (10 or 34 h). We collected whole transcriptome RNA-seq data derived from five animals at each dose and time point to perform a toxicogenomics analysis. Consistent with documented injury phenotypes for HgCl₂ toxicity, our kidney-injury-module approach identified the onset of necrosis and dilation as early as 10 h after a dose of 0.50 mg/kg that produced only mild injury as judged by urinary KIM-1 excretion. The results of these animal studies highlight the potential of the kidney-injury-module approach to provide a sensitive and histopathology-specific readout of renal toxicity.

1. Introduction

Kidney damage, which is a serious public health problem, is typically classified as either an acute kidney injury (AKI) or a chronic kidney disease (CKD) with a multifaceted etiology (Basile et al., 2016; Chevalier, 2016). AKI involves rapid deterioration of kidney function—a condition associated with a high mortality rate and can typically occur among patients in intensive care units (Blanco et al., 2019). Patients with CKD are often asymptomatic until two-thirds of the nephrons lose their function and, therefore, only diagnosed after the kidneys become severely damaged (López-Novoa et al., 2011). Another major cause of AKI and CKD cases in adults is drug-induced nephrotoxicity, which accounts for approximately 14–26% of all AKI cases

(Perazella, 2018). Both AKI and CKD are typically diagnosed only after symptoms manifest. Currently, available diagnostic tests include serum creatinine, urine microscopy, and urine output, are limited in their ability to identify early stages of kidney injury (Waikar et al., 2009, 2012). Hence, there is a continuous need to identify early injury markers, develop advance biomarker diagnostics, and improve treatment protocols (Han et al., 2002; Basile et al., 2016; Rizvi and Kashani, 2019). To assess the nephrotoxic risks of industrial chemicals or drugs under development in detail, we need to develop methods for the assessment of drug-induced kidney injury in either *in vitro* (cell) or *in vivo* (animal) studies.

The overall goal of our research is to develop computational and experimental methods by which we can assess chemically-induced

* Corresponding author at: DoD Biotechnology High Performance Computing Software Applications Institute, Telemedicine and Advanced Technology Research Center, U.S. Army Medical Research and Development Command, Fort Detrick, MD, USA.

** Corresponding author.

E-mail addresses: pschyman@bhsai.org (P. Schyman), masakazu.shiota@vanderbilt.edu (M. Shiota).

¹ These authors contributed equally to this work.

organ injuries in liver and kidney tissues, based on *in vitro* and *in vivo* exposure studies. Here, we performed low-dose acute *in vivo* animal exposures to a known kidney toxicant and compared different gene, pathway, and gene-module analysis methods in characterizing the transcriptomic response. In this context, the aim of the current study is to identify and interpret toxicant-induced genome-wide transcriptional changes and link them to a phenotypic description of known kidney injuries. Genome-wide gene-expression analysis is one of the most common approaches in studying the full range of cellular transcriptional responses induced by chemical perturbations (Hamadeh et al., 2002; Sahini et al., 2014; Ippolito et al., 2015; Parmentier et al., 2017). It is used in both liver- and kidney-specific analyses of pathways and selected gene sets in cultured cells (*in vitro*) and animal models (*in vivo*) (Segal et al., 2004; Fielden et al., 2005; Minowa et al., 2012; Sahini et al., 2014; Parmentier et al., 2017; Sutherland et al., 2019; Wang et al., 2019). We previously described a toxicogenomic approach to derive sets (modules) of co-expressed genes correlated with graded histopathology phenotypes (AbdulHameed et al., 2014; Ippolito et al., 2015; Te et al., 2016) by mining either the DrugMatrix (Ganter et al., 2005) or Open Toxicogenomics Project-Genomics Assisted Toxicity Evaluation System (TG-GATEs) (Igarashi et al., 2015) databases. This method further identifies the extent to which the degree of histopathologic injury is associated with the degree of fold change in the expression of the constituent genes induced via the activation of each injury module (i.e., the larger the fold change, the more severe the injury). The strength of this approach is that it allows us to correlate gene-expression responses with graded levels of histopathology-specific damage for both the liver and kidney. We have successfully applied the approach in both *in vitro* and *in vivo* experiments using small molecule exemplar chemicals with known liver-injury phenotypes (Ippolito et al., 2015; AbdulHameed et al., 2016; Te et al., 2016; McDyre et al., 2018; Schyman et al., 2018, 2019).

Mercuric chloride (HgCl_2) is an extremely toxic substance that is frequently used to model kidney injury (Thukral et al., 2005; Trebucobich et al., 2014; Tokumoto et al., 2018; Caglayan et al., 2019; Rojas-Franco et al., 2019). Upon exposure to HgCl_2 , highly reactive inorganic mercury ions rapidly accumulate primarily in the renal proximal tubular cells, which leads to tubular necrosis and, consequently, to AKI or CKD (Zalups, 2000; Miller et al., 2013; Elshemy et al., 2018). A single dose of 1 g can be fatal in an adult human, but toxicity can also accumulate over time. Although HgCl_2 is mainly metabolized in the liver, among the brain, liver, and kidneys, it shows the highest level of accumulation in the kidneys (Hussain et al., 1997). Kidney failure may occur within 24 h after HgCl_2 exposure, primarily because of necrosis of the tubular epithelium (Pollard and Hultman, 1997).

Here we present our first study focused on the kidney injury responses, using our previously developed kidney-injury modules. We used HgCl_2 as a model chemical for toxic kidney responses (Harbison, 1998), to induce mild exposures in rats and collect whole genome RNA-seq data for analysis. To induce very low to mild toxic kidney responses in rats, we treated different groups of rats with one of two doses: 1) a “high” dose—the lowest dose that resulted in detectable increases in levels of the liver-injury marker aspartate aminotransferase (AST) in plasma and kidney-injury molecule 1 (KIM-1) in urine (Han et al., 2002), and 2) a “low” dose—50 % of the high dose, which did not show any significant increases in AST levels, but did increase urinary KIM-1 levels. We performed the experiments to collect the kidney RNA-seq data for toxicogenomic analysis at two time points (10 and 34 h).

2. Materials and methods

2.1. Animals

All experiments were conducted in accordance with the Guide for the Care and Use of Laboratory Animals of the United States Department of Agriculture, the Vanderbilt University Institutional

Animal Care and Use Committee, and the U.S. Army Medical Research and Development Command Animal Care and Use Review Office. For our studies in animals, 8-week-old male Sprague Dawley rats were purchased from Charles River Laboratories (Wilmington, MA), they were housed three per cage and fed Formulab Diet 5001 (Purina LabDiet, Purina Mills, Richmond, IN) and had access to water *ad libitum*.

At 10 weeks of age and seven days prior to each experiment, we anesthetized the rats with isoflurane and surgically implanted a catheter as previously described (Shiota, 2012). For preliminary studies to determine the appropriate experimental conditions (dose and time after exposure), and for studies to measure changes in gene expression, we cannulated the right external jugular vein using a sterile silicone catheter with an inner diameter of 0.51 mm and an outer diameter of 0.94 mm, which was fixed to the back of the neck by passing its free end subcutaneously as previously described (Shiota, 2012). The catheter was used to collect blood to measure AST levels. Each catheter was occluded with a metal plug after flushing it with heparinized saline (200 U heparin/mL). Following surgery, rats were housed individually.

2.2. Preliminary study to optimization of mercuric chloride dose and length of exposure

Two days before each study, we moved each animal from its regular housing cage to a metabolic cage (Harvard Apparatus, Holliston, MA) where the animals were kept for the duration of the experiment. The protocol in Fig. 1A was followed to determine an appropriate dose of HgCl_2 and length of exposure. We divided 24 animals into 8 groups ($n = 3$ per dose), gave intraperitoneal (IP) injections of either vehicle (1 mL/kg of saline) or HgCl_2 (0.125, 0.25, 0.5, 1, 2, 4, or 8 mg/kg) at 9 a.m. Samples of blood (100 μL) collected from the jugular vein catheter and accumulated urine (urine produced between each collection time) was collected at 8, 24, 32, 48, and 56 h after each treatment dose. We administered either vehicle or HgCl_2 with a single IP injection immediately after an initial blood and urine collection at 9 a.m. on the first day and the animals had access to water and food *ad libitum* throughout the study. After collecting the last blood and urine samples, we euthanized the rats by intravenous (IV) administration of sodium pentobarbital (60 mg/kg) through the jugular vein and then harvested the kidneys. We measured standard biomarkers of liver and kidney injury in the blood and urine.

2.3. Measurement of toxicant-induced changes in gene expression

Based on the results of our optimization studies, we selected two doses (low and high) and two lengths of exposure. Six groups of five animals were assigned to receive saline, 0.25 mg/kg (low dose), or 0.5 mg/kg (high dose) of HgCl_2 and one of two exposure durations (10 or 34 h). We collected blood and tissue samples 10 or 34 h following treatment (Fig. 1B).

For all six treatment groups, we transferred each rat into a new housing cage at 7 a.m. and gave either an IP injection of vehicle or HgCl_2 . For the 10 h groups, we provided access to water *ad libitum* but no food prior to treatment. For the 34 h groups, we provided access to water and food *ad libitum* for 24 h; and then on the next day, we transferred each rat into a new housing cage at 7 a.m. and allowed access to water *ad libitum*, but no food. At 5 pm on day 1 for the 10 h groups and day 2 for the 34 h groups, following a blood sample collection, we anesthetized each animal with an IV injection of sodium pentobarbital (50 mg/kg) through the jugular vein catheter and immediately subjected the animal to a laparotomy. Urine was collected directly from the bladder, and kidneys were dissected and then frozen using Wollenberger tongs precooled in liquid nitrogen. The collected plasma, urine, and organ samples were stored in a -80°C freezer until needed for analyses.

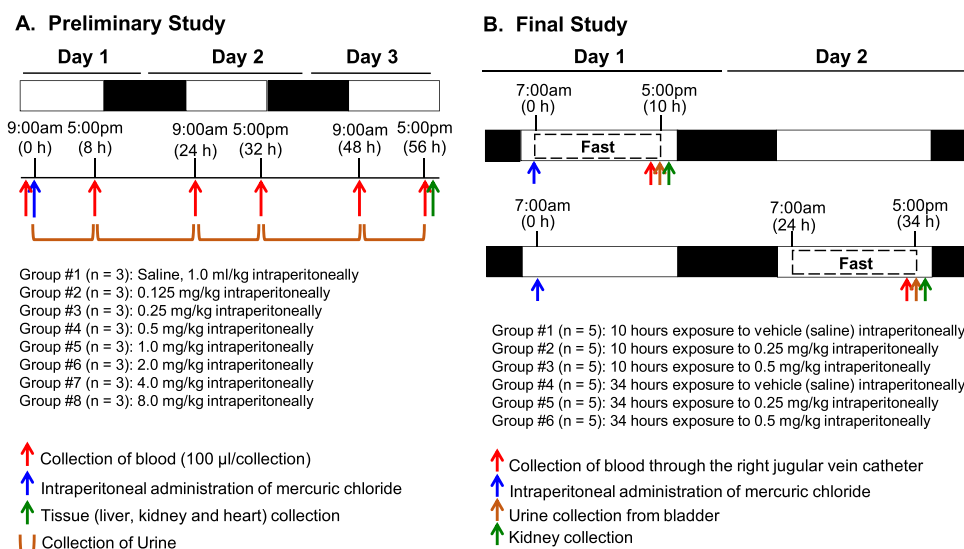


Fig. 1. Protocol for optimizing mercuric chloride doses for sub-acute toxicity. Protocol for single intraperitoneal (IP) administration of mercuric chloride in Sprague Dawley rats for (A) optimizing dose and time after exposure for assessment and (B) measuring changes in gene expression.

2.4. Measurement of tissue injury markers in blood and urine

We measured plasma AST activity and KIM-1 concentration in urine using an AST activity assay kit (Sigma-Aldrich, St Louis, MO) and a KIM-1 Rat ELISA kit (Abcam Inc., Cambridge, MA), respectively.

2.5. RNA isolation and sequencing

Given the histological heterogeneity of kidneys, we powdered the frozen whole kidneys in liquid nitrogen and isolated total RNA using TRIzol Reagent (Thermo Fisher Scientific, Waltham, MA) and the direct-zol RNA MiniPrep kit (Zymo Research, Irvine, CA). These RNA samples were then submitted to the Vanderbilt University Medical Center VANTAGE Core (Nashville, TN) for RNA quality determination and sequencing. To assess total RNA quality, a 2100 Bioanalyzer (Agilent, Santa Clara, CA) was used. Starting with at least 200 ng of DNase-treated total RNA of high RNA integrity, poly-A-enriched mRNA libraries were generated using KAPA Stranded mRNA sample kits with indexed adaptors (Roche, Indianapolis, IN). The libraries were assessed for quality using a 2100 Bioanalyzer (Agilent) and quantitated using KAPA library Quantification kits (Roche). In accord with the manufacturer's protocol, libraries were subjected to 75-bp paired-end sequencing (Illumina HiSeq3000, San Diego, CA). The Bcl2fastq2 Conversion Software (Illumina) was used to generate de-multiplexed Fastq files.

2.6. Analysis of RNA-seq data

We used the RNA-seq data analysis tool Kallisto for read alignment and quantification (Bray et al., 2016). Kallisto pseudo-aligns the reads to a reference, producing a list of transcripts that are compatible with each read while avoiding alignment of individual bases. In this study, we pseudo-aligned the reads to the *Rattus norvegicus* transcriptome (Rnor_6.0 release-91) downloaded from the Ensemble website (<http://www.ensembl.org/index.html>) (Zerbino et al., 2018). We employed the bootstrapping technique to calculate uncertainties of transcript abundance estimates by repeating the analyses 100 times after resampling with replacement. Interested readers may access the files from the RNA-seq analysis deposited in NCBI's Gene Expression Omnibus (GEO) database, using GEO series accession number GSE147248.

To identify significantly expressed genes from transcript abundance data, we used Kallisto's companion analysis tool Sleuth, which uses the results of the bootstrap analysis during transcript quantification to

directly estimate the technical gene variance for each sample (Pimentel et al., 2017). We defined a significantly expressed gene as one with a false discovery rate adjusted p-value (q-value) of no more than 0.05 and a differentially expressed gene (DEG) as one with a false discovery rate adjusted p-value (q-value) of no more than 0.05 and a relative fold change (FC) value larger than a factor of 2 ($|\log_2(\text{FC})| > 1$). In the Supplemental Material, we provide the q-values and FC values.

2.7. The aggregate fold change method

We previously developed the aggregate FC (AFC) and the aggregate absolute FC (AAFC) methods to identify gene sets that significantly change between treatment and control cohorts (Schyman et al., 2018, 2019). The AFC method is useful for pathway analysis as it takes into account the directionality of gene expression, i.e., whether a pathway is up- or down-regulated. In contrast, the AAFC method provides a measure of how much a set of genes is disrupted regardless of whether the genes are over- or under-expressed. It is particularly useful for analyzing a group of genes that are mechanistically unrelated, (e.g., our kidney injury modules). Both the AFC and AAFC methods first calculate the FC value for each gene, i.e., the difference between the mean log-transformed gene-expression values for samples in the treatment and control cohorts. Subsequently, the AFC method calculates the total FC value for each gene set by taking the log-transformed FC value for each gene, whereas the AAFC method does so by taking the absolute value for each gene.

We then used the module scores to perform null hypothesis tests and to estimate the significance of each module by its p-value, defined as the probability that the score for randomly selected FC values (repeated 10,000 times) is greater than the score from the actual module. A small p-value (< 0.05) implies that the module value is significant. The z-score is the number of standard deviations by which the actual module value differs from the mean of the randomly selected FC values (repeated 10,000 times). As such, it indicates the degree of module activation (i.e., the module activation score) and can be used to rank the modules.

3. Results

3.1. Optimization of mercuric chloride doses for sub-acute toxicity

In rats, a single IP injection of HgCl_2 at a dose ranging from ~ 3 to 9 mg/kg (Lund et al., 1993; Wilks et al., 1994; Yanagisawa et al., 1998;

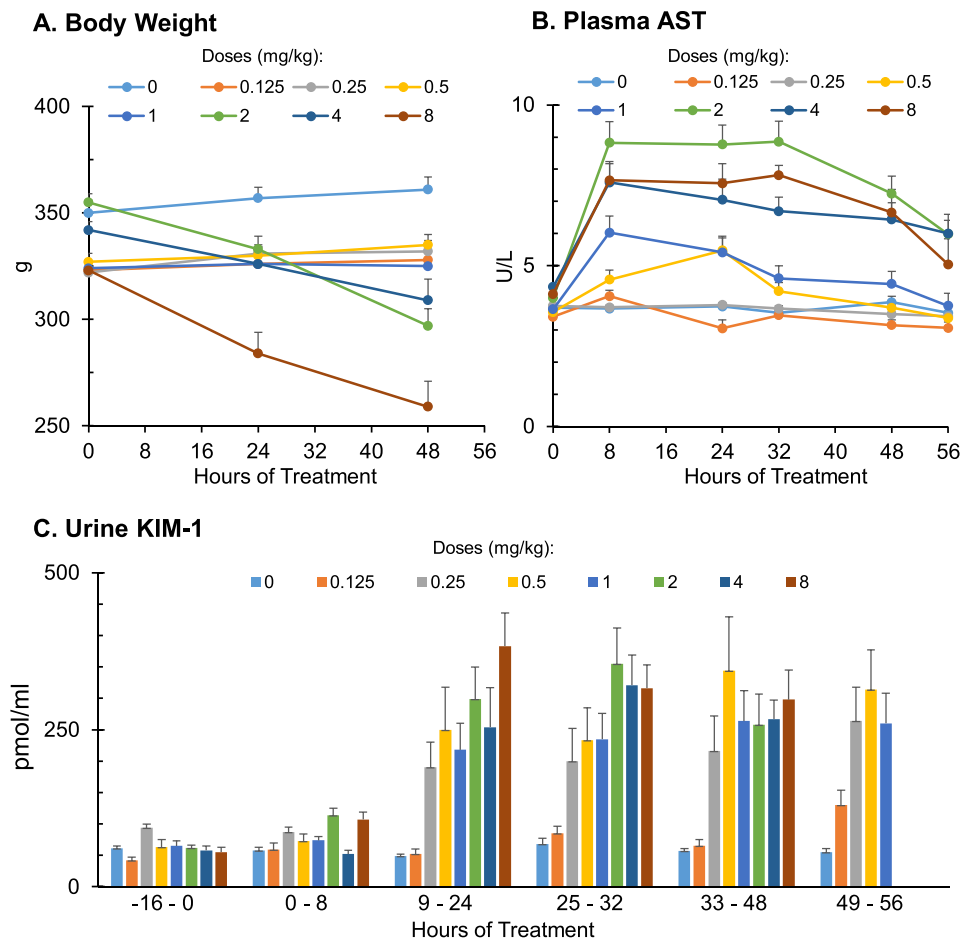


Fig. 2. Measurements of injury markers. Effect of a single intraperitoneal (IP) injection of mercuric chloride on (A) body weight, (B) plasma aspartate aminotransferase (AST), and (C) urine kidney-injury molecule-1 (KIM-1).

Table 1

Measured plasma AST and urine KIM-1 levels in the study to measure HgCl₂-induced changes in gene expression. Data are presented as the mean value with the corresponding standard deviation (SD) (n = 5 per dose).

HgCl ₂ dose		10 h				34 h			
Level	Concentration	AST (U/L)	SD	KIM-1 (pg/mL)	SD	AST (U/L)	SD	KIM-1 (pg/mL)	SD
Vehicle	0.00 mg/kg	3.61	0.27	55.00	9.41	3.57	0.14	54.20	7.66
Low	0.25 mg/kg	3.53	0.28	65.80	14.58	3.53	0.21	205.00	34.20
High	0.50 mg/kg	4.57	0.76	70.00	8.00	4.11	0.19	218.20	51.32

Perottoni et al., 2004; Augusti et al., 2008; Hazelhoff et al., 2012; Joshi et al., 2017) causes renal injury within 3 h to 4 days after dosing, as shown by elevated plasma levels of urea, uric acid, creatinine, and blood urea nitrogen, accompanied by histological changes, such as necrosis and degenerated renal tubules with obstructed lumina. Our goal was to find a dose and a duration of exposure after dosing that would reveal detectable injury in the kidney within five days without the development of severe secondary complications.

We tested separate groups of rats (n = 3 each) at 8 different doses of HgCl₂ (i.e., 0 [vehicle], 0.125, 0.25, 0.5, 1.0, 2.0, 4.0, or 8.0 mg/kg). As shown in Fig. 2A, rats dosed at 0.125, 0.25, 0.5, or 1.0 mg/kg retained their body weight, suggesting that these doses did not affect eating. The dose of 0.125 mg/kg did not alter plasma AST or urine KIM-1 levels during the test period (Fig. 2B and C). The dose of 0.25 mg/kg did not alter plasma AST levels during the test period but elevated urine KIM-1 levels between 9–24 h of dosing. For rats dosed at 0.50 mg/kg, plasma AST levels became slightly higher than those in vehicle-treated rats within 24 h, whereas urine KIM-1 levels increased between 9–24 h of

dosing. In rats dosed at 1.0 mg/kg, plasma AST levels increased by 50 % within 8 h and urine KIM-1 levels increased markedly between 9–24 h of dosing. Rats dosed at 2, 4, and 8 mg/kg lost between 10 % and 18 % of their body weight, showed a marked increase in plasma AST levels within 8 h and urine KIM-1 levels between 9–24 h of dosing.

This preliminary study indicates that an IP injection of the doses (0.25, 0.50, and 1.0 mg/kg) of HgCl₂ leads to some physical injury of the kidneys without any loss of body weight or development of severe secondary complications. Therefore, for the final study (Fig. 1B), we gave each subject a single IP injection at one of two doses (0.25 mg/kg [low dose] or 0.50 mg/kg [high dose]) and one of two assessment times after dosing (10 or 34 h). Table 1 shows the AST and KIM-1 levels of the final study. We did not note any significant changes in AST levels compared with the control groups at either low or high doses within 10 or 34 h, which suggests no liver injury. At 10 h, we observed an increasing trend in the KIM-1 levels for the low and high doses of HgCl₂, but changes were within the standard deviations. However, within 34 h after low and high doses, the KIM-1 levels were significantly elevated

Table 2
Number of DEGs in rat kidney at a fixed q-value of less than 0.05 and different relative fold changes (FCs).

HgCl ₂ dose	10 h		34 h	
	$ \log_2(\text{FC}) > 0$	$ \log_2(\text{FC}) > 1$	$ \log_2(\text{FC}) > 0$	$ \log_2(\text{FC}) > 1$
Level Concentration				
Low 0.25 mg/kg	22	5	88	10
High 0.50 mg/kg	134	10	10	7

compared to their respective control groups.

3.2. Transcriptome analysis

We performed RNA-seq analysis by comparing transcript abundance levels in the kidneys between rats treated with vehicle (control) and those treated with HgCl₂ (0.25 mg/kg or 0.50 mg/kg) at 10 h or 34 h after dosing. Table 2 summarizes the number of significantly differentially expressed genes (DEGs) based on a fixed q-value of less than 0.05 and different relative fold changes (FCs), *i.e.*, any fold change value ($|\log_2(\text{FC})| > 0$) or a fold change value larger than a factor of 2 ($|\log_2(\text{FC})| > 1$). At the low doses selected, there were no obvious dose or time dependence in the number of DEGs. The relatively low number of DEGs is also commensurate with a relatively benign early toxic response.

The DEGs for each dose and exposure length compiled based on the $|\log_2(\text{FC})| > 1$ -fold change criterion in expression levels are shown in Table 3. The majority of DEGs (80 %) were downregulated at the early time point (10 h), whereas all DEGs except one were upregulated at the later time point (34 h) regardless of the dose. Although the trend of

overall downregulation followed by upregulation was the same for both dose regimens, there was no overlap among the top DEGs between the studied conditions. However, with only a few DEGs the chance of identifying overlapping genes between conditions is low. This is one of the issues using single gene identifiers.

The extensive literature on the toxic effects of mercury and HgCl₂ on the kidney (Fowler, 1993; Harbison, 1998; Barbier et al., 2005) allowed us to map the observed transcript changes to proposed injury mechanisms (Rojas-Franco et al., 2019). Systemic response mechanisms also encompass gene and transcript changes that occur in other organs, such as the liver, brain, and testes, which typically appear after prolonged low-level exposures and accumulations. These mechanisms also depend on the dose, route of administration, and time and duration of exposure, as well as sex- and age-specific responses among other factors (Oliveira et al., 2017).

The clear separation of the early downregulation of the overall transcriptomic response in the 10 h high-dose group is consistent with the view that downregulation of transcription is a general cellular response to stress, such as when *E. coli* transcriptomes show an initial preferential downregulation of genes (LaVoie and Summers, 2018). The most coherent transcriptional change was the upregulation of genes in the 34 h high-dose group, which indicated an increase in the xenobiotic stress response (*Ephx1*, *Ugt2b35*, *Gstp1*, and *Abcc2*, indicated in italics in Table 3). In addition, the DEGs involved in cell death (*Pcsk9*, *Mmp9*, *Stra6*, *Sncap*, *Clip3*, *Adcyap1r*, *Slc2a3*, *Ryr2*, *Ndnf*, and *Gstp2*, indicated in bold font in Table 3) and cytoskeletal development (*Krt79*, *Mmp9*, *Clip3*, *Dock10*, *Syne4*, and *Odf2*, indicated by a dagger in Table 3) for all dose and time groups, albeit not in a manner that made the functional relevance of each change readily apparent, suggested enhanced cell death and disrupted cytoskeletal development. These findings are consistent with previous work showing that, enhanced cell death, disrupted cytoskeletal development, and xenobiotic metabolism are all associated with exposure to mercury (Harbison, 1998). The mild doses

Table 3
Differentially expressed genes (DEGs) in the rat kidney after HgCl₂ treatment. Criteria to identify a DEG: q-value of less than 0.05 and an absolute log₂ fold-change value greater than 1.

10 hours				34 hours			
[Low]		[High]		[Low]		[High]	
Gene	log ₂ (FC)	Gene	log ₂ (FC)	Gene	log ₂ (FC)	Gene	log ₂ (FC)
Upregulation							
				Sncap	7.4		
				<i>Zfp523*</i>	6.2		
				Clip3 †	5.1	<i>Odf2</i> †	5.2
				Adcyap1r1	5.1		
				<i>Dock10</i> †	4.2	Ndnf	3.7
				Slc2a3	3.5	<i>Ephx1</i>	3.0
		<i>Ankrd66</i>	1.5	<i>Syne4</i> †	1.6	<i>Csmd1</i>	1.9
						<i>Ugt2b35</i>	1.4
<i>Fam166a</i>	1.3			<i>Rc3h2*</i>	1.2	<i>Gstp1</i>	1.3
<i>Gabbr2</i>	1.1			<i>Fsd11*</i>	1.1	<i>Abcc2</i>	1.1
Downregulation							
<i>Krt79</i> †	-1.1	<i>Mmp9</i> †	-1.0				
<i>Mbl1</i>	-1.2	<i>Stra6</i>	-1.0				
<i>Pcsk9</i>	-1.3	<i>Slc24a3</i>	-1.2				
		<i>Mylk3</i>	-1.2				
		<i>Ebf2*</i>	-2.1				
		<i>Porfl</i>	-2.7				
		<i>Ucp1</i>	-3.8				
		<i>Rfx4*</i>	-4.2				
		<i>Aff3*</i>	-4.7	<i>Ryr2</i>	-4.7		

Bold, cell death; *Italicized*, xenobiotic; *, transcription; †, cytoskeletal development annotations from the Rat Genome Database (Smith et al., 2020). Dose of HgCl₂ treatment: Low, 0.25 mg/kg; High, 0.50 mg/kg.

used in this study did not allow us to capture the elevated levels of heat shock proteins seen within 24 h after a single IP injection of 3.5 mg/kg of HgCl₂ (Stacchiotti et al., 2004), although *Hsp72* transcript levels were elevated in our study, albeit non-significantly (data not shown).

Many of the previously mentioned genes (*Gstp1*, *Abcc2*, *Ugt2b35*, *Ephx1*, *Slc2a3*, and *Mmp9*) are relevant to AKI (Imig, 2005; Shin et al., 2018). Shin et al. showed that increased expression of *Gstp1* in the kidneys of rats exposed to mercury is correlated with cytotoxicity (Shin et al., 2018). Consistent with the view that transporters play a role in mercury-induced nephrotoxicity (Barnett and Cummings, 2018), here we found that a glucose transporter (*Slc2a3*) and an ATP binding cassette transporter (*Abcc2*) were upregulated 34 h after administration of the low dose and high dose, respectively, of HgCl₂. In addition, 34 h after the high-dose treatment, we found upregulation of *Ephx1* (which can increase inflammation), consistent with a prior study showing that inhibition of *Ephx1* can have renal protective effects (Imig, 2005). Furthermore, 10 h after the high-dose treatment, we observed downregulation of *Mmp9*, which has been linked to increased apoptosis and delayed renal recovery (Bengatta et al., 2009), and downregulation of *Stra6*, which reportedly causes apoptosis and fibrosis of the kidneys (Chen et al., 2016).

3.3. KEGG pathway analysis

We used the AFC method (Ackermann and Strimmer, 2009) to identify significantly downregulated/upregulated pathways. For our analysis, we used the Kyoto Encyclopedia Gene and Genomes (KEGG) pathways (Kanehisa and Goto, 2000). Table 4 lists the KEGG pathways we identified as significantly altered (p-value < 0.01) 10 or 34 h after low-dose (0.25 mg/kg) or high-dose (0.50 mg/kg) treatment. Downregulated and upregulated pathways are highlighted in green and red, respectively, with the significance of the change indicated by the z-score as calculated according to the AFC method.

A genome-wide transcriptional analysis based on cellular processes and pathways provides for a more coherent interpretation of the results than does one based solely on genes. Specifically, compared with a gene-based analysis, a pathway-based analysis revealed a greater degree of overlap among affected pathways. Overall, the pathway analysis results were compatible with the results obtained by analyzing individual gene transcripts: downregulation at the earlier time point and upregulation at the later time point. Downregulation had major effects on multiple cellular- and immune-signaling pathways, consistent with work showing that inflammation and immune responses are closely involved in the pathogenesis of kidney injuries (Akcaay et al., 2009). The initial downregulation of pathways (e.g., the complement and coagulation cascades) at the earlier time point (10 h) for both low- and high-dose groups could represent an adaptive protective response to mercury exposure. For the high-dose group, upregulation of the complement and coagulation cascades, the TNF signaling pathway, and the chemokine signaling pathway at the later time point (34 h) is in general agreement with known AKI pathophysiology. In particular, upregulation of the complement and coagulation cascades for both dose groups is commensurate with the initiation of kidney injury.

Table 4 shows that not all of the significantly altered pathways were necessarily downregulated at the early time point, as were the transcriptional regulation of individual genes and the overall regulation of both genes and pathways. For example, a linked translational/ribosomal pathway, involving the *Spliceosome*, *Ribosome*, and *RNA transport* pathways, showed strong upregulation at the 10 h time point after high-dose treatment, which largely subsided at the 34 h time point.

We also endeavored to associate the affected pathways with a known renal mechanism of mercury-induced toxicity in a dose- and time-dependent manner (Zalups, 2000; Miller et al., 2013; Elshemy et al., 2018). Significantly upregulated pathways, such as the *ECM-receptor interaction*, *cell adhesion molecule*, *focal adhesion*, and *regulation of actin cytoskeleton* pathways, represent molecular processes associated

with AKI (Basile et al., 2012; Bachir et al., 2017). Previous studies have reported that alterations in basement membrane attachment, cytoskeletal structure, and distribution of cell adhesion molecules, which lead to loss of cell-cell contacts, constitute molecular mechanisms underlying AKI (Sharfuddin and Molitoris, 2011; Correa-Costa et al., 2012; Pozzi and Zent, 2013; AbdulHameed et al., 2016). Notably, in our model of mercury toxicity, this signal was largely absent at the low dose, whereas it was time-dependent at the high dose (i.e., an initial overall downregulation at 10 h followed by upregulation at 34 h). A consistent signal in the data was the overexpression of pathways related to cellular metabolism and the metabolism of xenobiotics. In addition to the liver, the kidneys play an important role in xenobiotic metabolism and the processing of endogenous metabolites (Bajaj et al., 2018). In our study, this response depended on both time and dose, reflecting the ongoing and developing reaction to HgCl₂ exposure. The upregulation of multiple pathways related to the metabolism, signaling, growth, and death of cells was strongest at 34 h after high-dose treatment. The only pathway significantly suppressed after high-dose treatment was that of oxidative phosphorylation.

3.4. Analysis based on kidney-injury modules

Previously, we derived eight kidney-injury modules (co-expressed gene sets) associated with specific histopathological kidney-injury phenotypes (Te et al., 2016). These modules are not curated injury pathways, but rather specific sets of genes co-expressed in response to a wide range of chemicals administered at various doses to induce kidney injuries in Sprague Dawley rats. As such, gene membership between modules can overlap and multiple modules can be activated by a particular chemical exposure condition. An important aspect of an injury module is that the change in its expression level is correlated with the degree of injury (i.e., a low/high activation score is indicative of a mild/severe histopathology score) (Te et al., 2016).

Table 5 shows activation scores (z-scores calculated by the AAFC method; See Method Section) for the kidney-injury modules at the two HgCl₂ doses and two assessment times after treatment. There was no significant module activation with the low dose (0.25 mg/kg) at either 10 or 34 h after treatment. At the high dose (0.50 mg/kg), the z-scores for the *Necrosis* and *Dilation* injury modules respectively increased to 2.3 and 2.7 at 10 h and to 5.9 and 7.0 at 34 h, revealing a dose-dependent increase in injury likelihood. The kidney-injury signals further intensified at 34 h, with the additional activation of the *Degeneration* and *Casts* injury modules. These modules are related to the general class of cellular and tissue degeneration processes closely associated with the pathology of kidney necrosis (Frazier et al., 2012).

Previous studies of HgCl₂ toxicity using IP injections in rodent models have shown that the kidney histopathology phenotypes described above are more likely to develop when the time after exposure is longer at comparable doses or when the dose is higher at comparable times after exposure (Thukral et al., 2005; Trebucovich et al., 2014; Tokumoto et al., 2018; Caglayan et al., 2019; Rojas-Franco et al., 2019). For example, Thukral et al. (Thukral et al., 2005) subjected male Sprague Dawley rats to 0.4–1.5 mg/kg of HgCl₂ and found tubular degeneration, casts, and necrosis on days 3 and 7, but not on day 1. Conversely, Trebucovich et al. (Trebucovich et al., 2014) found that injecting male Wistar rats with 4 mg/kg of HgCl₂ caused dilatation within 18 h.

To track kidney injuries before the appearance of histopathology phenotypes, we used relative KIM-1 protein levels in the urine and fold-change values of KIM-1 gene (*Havcr1*) expression levels in the kidneys to anchor nascent injuries to injury-module activation (Table 5). These measures showed a similar trend, with lower levels at 10 h and a marked increase at 34 h for both low- and high-dose treatments of HgCl₂. Although the fold-change values for *Havcr1* were above 2, the false discovery rate did not flag this gene as having a significant DEG in Table 3. Similar to levels of module activation, KIM-1 protein levels

Table 4

KEGG pathways identified as significantly altered using the aggregate fold-change method and gene-expression data after exposure to HgCl₂. Dose of HgCl₂ treatment: Low, 0.25 mg/kg; High, 0.50 mg/kg.

Physiological Processes & Pathways	10 hours		34 hours	
	[Low]	[High]	[Low]	[High]
Metabolism				
	z-score			
Drug metabolism - CYP450			4.6	4.9
Metabolism of xenobiotics by CYP450	3.9		4.8	4.6
Porphyrin and chlorophyll metabolism	3.3	2.8		5.1
Ascorbate and aldarate metabolism				4.5
Pentose and glucuronate interconversions			4.8	4.5
Retinol metabolism			8.1	4.3
Linoleic acid metabolism	-3.7	-3.8	4.3	
Steroid hormone biosynthesis	-4.0		7.7	
Arginine biosynthesis	-4.1			
Lysine degradation		-2.8		
Tyrosine metabolism			4.2	
Nitrogen metabolism	-3.0			
Oxidative phosphorylation		3.3	-3.7	-3.6
Cytoskeleton & Trafficking				
Regulation of actin cytoskeleton	3.0			2.8
Protein processing in endoplasmic reticulum		3.5		
Adherens junction		-2.8		3.0
Focal adhesion		-3.2	3.3	3.5
Vascular smooth muscle contraction		-2.7		
Cell adhesion molecules (CAMs)		-3.1		3.4
ECM-receptor interaction		-3.8		3.7
Peroxisome	-3.9			
Cell Cycle/Transcription				
Cell cycle				3.0
Spliceosome		4.9		
Ribosome biogenesis in eukaryotes		4.7		
RNA transport		3.5		
Ribosome		3.2	-5.2	
Base excision repair			-3.7	
Cell & Immune Signaling				
Complement and coagulation cascades	-8.0	-7.2	5.9	6.9
PPAR signaling pathway	-3.7	-6.5	2.9	
PI3K-Akt signaling pathway		-3.0		2.9
TNF signaling pathway				3.8
Chemokine signaling pathway				2.8
Platelet activation		-3.2		
Glucagon signaling pathway		-3.2		
Insulin signaling pathway		-3.3		
Regulation of lipolysis in adipocytes		-4.0		
Cholinergic synapse		-3.2		
Glutamatergic synapse		-2.9		
Serotonergic synapse		-2.8		
AMPK signaling pathway		-2.8		
Apelin signaling pathway	-3.8		-3.6	
cAMP signaling pathway			-2.9	
cGMP-PKG signaling pathway			-2.9	
Hedgehog signaling pathway			-3.0	
Rap1 signaling pathway			-2.9	
Digestion & Absorption				
Primary bile acid biosynthesis	-4.5			
Bile secretion			-3.9	3.1
Fat digestion and absorption			-3.4	
Gastric acid secretion			-3.1	
Protein digestion and absorption			-3.7	
Salivary secretion			-3.1	

Table 5
Activation of kidney-injury modules and expression levels of the KIM-1 gene and protein after HgCl₂ exposure.

Kidney-Injury Module	10 hours		34 hours	
	[Low]	[High]	[Low]	[High]
Degeneration				
Necrosis	-1.0	2.3	0.4	7.0
Dilatation	-0.8	2.7	1.1	5.9
Degeneration	-1.4	-0.5	-0.9	5.9
Casts (hyaline)	-1.8	1.1	-1.3	5.2
Inflammation				
Fibrogenesis	-2.7	-2.2	-3.0	1.9
Cellular infiltration	-1.9	-0.6	-1.2	0.9
Intracytoplasmic inclusion body	-1.3	0.3	-1.9	-1.7
Proliferation				
Hypertrophy	0.0	1.7	-0.1	-0.1
Kidney Injury Molecule 1				
KIM-1 (Havcr1 gene expression, fold change)	1.1	1.9	3.0	8.7
KIM-1 (relative protein level)	1.2	1.3	3.8	4.0

Quantities in **bold** indicate significant activation of modules (*i.e.*, z-scores greater than two standard deviations). Dose of HgCl₂ treatment: Low, 0.25 mg/kg; High, 0.50 mg/kg.

were highest at 34 h for the high dose HgCl₂ treatment. Module activation was greatest for degeneration processes associated with the *Necrosis*, *Dilatation*, *Degeneration*, and *Casts* modules, consistent with the nascent development of these histopathology phenotypes (Thukral et al., 2005; Trebucobich et al., 2014; Tokumoto et al., 2018; Caglayan et al., 2019; Rojas-Franco et al., 2019). At the low dose, our injury-module analysis did not identify any significantly activated module, although KIM-1 protein levels were elevated 34 h after treatment as they were at the high dose. In contrast, 10 h after high-dose treatment, z-scores increased by more than two standard deviations for the *Necrosis* and *Dilation* modules, whereas the relative change in KIM-1 levels was 1.3.

4. Discussion

An extensive literature on the toxicity induced by HgCl₂, using a wide range of doses and assessment times following chemical exposure, indicates that damage to kidney tissues, resulting in systemic acute renal failure and severe histopathology, occurs with dose-dependent severity only after a considerable delay (Stacchiotti et al., 2003). Here, we aimed to assess the ability of our kidney-injury modules to correctly identify nascent damage at the lowest toxicity levels and earliest times after exposure. To this end, we calibrated our animal studies to contrast a control group with two groups given relatively low doses (0.25 or 0.50 mg/kg) of HgCl₂, and assessed the effects 10 or 34 h after exposure (when we expected neither systemic acute renal failure nor the development of severe histopathology). We identified nascent kidney injuries by the absence and presence of elevated KIM-1 protein levels in the urine at 10 and 34 h after HgCl₂ exposure, respectively. Given that both AST and KIM-1 levels decreased at the most delayed assessment time after exposure in all preliminary studies, we expect that these injuries can be reversed to restore the kidneys to their normal state. The ability to prospectively predict injury phenotypes using sub-acute toxic doses can circumvent systemic contributions due to secondary complications of mercury poisoning from obscuring the kidney response.

We used genome-wide RNA-seq datasets collected for each dose and time point to initially perform standard differential gene-expression and pathway-enrichment analyses. However, at these toxicity levels we could only detect a few DEGs (Table 2) without overlapping gene

signals from the four study points. The transcriptional response was primarily time-dependent, with a general downregulation of gene transcription at 10 h and a transcriptionally encoded upregulated response at 34 h, regardless of dose. Given the extensive literature on the mechanisms of HgCl₂ toxicity, we were able to link the DEGs to cellular processes, such as cell death, xenobiotic metabolism, and cytoskeletal development (Table 3). The measured protein level of the biomarker KIM-1 in urine, which correlated with the expression level of the KIM-1 (Havcr1) gene, readily tracked kidney injury after 34 h. Although Havcr1 expression levels tracked KIM-1 levels, the presence of the Havcr1 gene expression in the kidneys never met our false discovery rate criteria.

Even though only a small number of genes were qualified as DEGs, many genes could still be changing. The method we used to calculate a gene-set score for pathways and modules is to sum all gene-fold change values in the set, and compare it to the sum of randomly selected genes. In this way, many small contributions in a set (co-expression) may become significant. This is one of the reasons gene set approaches could provide a more robust signal than relying solely on single gene identifications.

To identify physiological processes and pathways associated with toxicity from the exposure data, we performed KEGG-pathway enrichment analysis using the entire RNA-seq dataset. The general trend was similar to that from the DEG analysis: an overall downregulation at 10 h and an overall upregulation at 34 h. However, the implications were more multifaceted with several exceptions, including upregulation of pathways linked to xenobiotic metabolism at 10 h and downregulation of oxidative phosphorylation at 34 h. As was the case for the analysis based on individual genes, we were able to link the altered pathways to processes and mechanisms previously associated with HgCl₂ toxicity, the key kidney-injury phenotype of which is tubular necrosis (Pollard and Hultman, 1997). The analysis revealed that HgCl₂ triggered a cascade of gene transcription events, which strongly activated several pathways important for necrosis and inflammation at 34 h (Table 4): the *Complement and coagulation cascade* and *Chemokine signaling* pathways, which are important for inflammatory processes; the *Tumor Necrosis Factor (TNF) signaling* and *Cell cycle* pathways, which are critical in a wide range of signaling pathways, including apoptosis and inflammation; and the *Extracellular matrix (ECM) receptor*, *Focal adhesion*,

and *Cell adhesion molecules (CAMs)* pathways, which are involved in cellular processes, such as proliferation, apoptosis, and adhesion.

We previously developed an approach to identify kidney-injury modules that represent sets of genes correlated with specific injury phenotypes (Te et al., 2016). These modules and their activation by transcriptome data allow us to annotate specific injury phenotypes. In this study, module activation by HgCl₂ intensified as the injury progressed over time, resulting in the strongest signal at 34 h after high-dose exposure (Table 5). The injury modules significantly activated under these conditions (*Necrosis, Dilatation, Degeneration, and Casts [hyaline]*) were consistent with the known phenotypes of acute HgCl₂ toxicity, i.e., marked localized necrosis, dilatation, and casts. Activation of these modules was dose-dependent, as they were not significantly activated at the low dose. Notably, injury-module activation was correlated with experimentally measured KIM-1 levels (Table 5), suggesting that the former could serve as an early signal of impending kidney injury when analyzing gene expression samples.

Finally, chronic exposure to HgCl₂ eventually leads to fibrosis (Elshehy et al., 2018). Although we did not assess how varying the duration of HgCl₂ exposure would affect injury modules in this study, the injury-module analysis showed that activation of the *Fibrogenesis* module increased by almost two standard deviations compared to the control condition 34 h after high-dose treatment with HgCl₂ (Table 5). This finding suggests that the injury modules used here may also serve as indicators of impending kidney injuries following HgCl₂ exposure.

5. Conclusion

Physical injuries, diseases, and exposure to harmful toxicants can all cause kidney damage, depress renal function, and potentially death. Apart from acute renal failure, the resilience of the kidney in maintaining renal function can mask injuries to the organ, leaving the underlying cause untreated. We aim to develop experimental and computational modeling techniques to ascertain the potential of chemicals to cause kidney damage. Injury-module analysis provides a means to interpret toxicant-induced changes in transcriptomes based on phenotypic descriptions of kidney injuries. This method offers a coherent injury representation with an explanatory power beyond that of differentially expressed genes or pathway-enrichment analyses. Although its general applicability to a variety of means of causing kidney damage remains to be demonstrated, the injury-module approach captured key elements of HgCl₂ poisoning. This points the way forward to future studies that exploit injury-module activation as a sensitive tool to capture chemical toxicity, predict outcomes for potential tissue damage, and mine the outcomes for alternative biomarker panels as well as ways to bridge animal/human studies and *in vitro* studies.

CRediT authorship contribution statement

Patric Schyman: Conceptualization, Data curation, Formal analysis, Investigation, Methodology, Software, Writing - original draft, Writing - review & editing. **Richard L. Printz:** Conceptualization, Investigation, Methodology, Validation, Writing - review & editing. **Mohamed Diwan M. AbdulHameed:** Conceptualization, Investigation, Writing - review & editing. **Shanea K. Estes:** Investigation. **Chiyo Shiota:** Investigation. **Masakazu Shiota:** Conceptualization, Investigation, Methodology, Validation, Writing - review & editing. **Anders Wallqvist:** Conceptualization, Methodology, Writing - review & editing.

Declaration of Competing Interest

The authors declare no conflicts of interest.

Acknowledgments

The authors were supported by the U.S. Army Medical Research and Development Command (Fort Detrick, MD, USA), and the Defense Threat Reduction Agency grant CBCall14-CBS-05-2-0007. The opinions and assertions contained herein are the private views of the authors and are not to be construed as official or as reflecting the views of the U.S. Army, the U.S. Department of Defense, or The Henry M. Jackson Foundation for Advancement of Military Medicine, Inc. The Vanderbilt University Medical Center VANTAGE Core provided technical assistance for RNA sequencing. VANTAGE is supported in part by CTSA Grant (SUL1 RR024975-03), the Vanderbilt Ingram Cancer Center (P30 CA68485), the Vanderbilt Vision Center (P30 EY08126), and NIH/NICRR (G20 RR030956). This paper has been approved for public release with unlimited distribution.

References

- AbdulHameed, M.D.M., Tawa, G.J., Kumar, K., Ippolito, D.L., Lewis, J.A., Stallings, J.D., et al., 2014. Systems level analysis and identification of pathways and networks associated with liver fibrosis. *PLoS One* 9, e112193. <https://doi.org/10.1371/journal.pone.0112193>.
- AbdulHameed, M.D.M., Ippolito, D.L., Stallings, J.D., Wallqvist, A., 2016. Mining kidney toxicogenomic data by using gene co-expression modules. *BMC Genomics* 17, 790. <https://doi.org/10.1186/s12864-016-3143-y>.
- Ackermann, M., Strimmer, K., 2009. A general modular framework for gene set enrichment analysis. *BMC Bioinform.* 10, 47. <https://doi.org/10.1186/1471-2105-10-47>.
- Akcaay, A., Nguyen, Q., Edelstein, C.L., 2009. Mediators of inflammation in acute kidney injury. *Mediators Inflamm.* 2009, 137072. <https://doi.org/10.1155/2009/137072>.
- Augusti, P.R., Conterato, G.M.M., Somacal, S., Sobieski, R., Spohr, P.R., Torres, J.V., et al., 2008. Effect of astaxanthin on kidney function impairment and oxidative stress induced by mercuric chloride in rats. *Food Chem. Toxicol.* 46, 212–219. <https://doi.org/10.1016/j.fct.2007.08.001>.
- Bachir, A.I., Horwitz, A.R., Nelson, W.J., Bianchini, J.M., 2017. Actin-based adhesion modules mediate cell interactions with the extracellular matrix and neighboring cells. *Cold Spring Harb. Perspect. Biol.* 9, a023234. <https://doi.org/10.1101/cshperspect.a023234>.
- Bajaj, P., Chowdhury, S.K., Yucha, R., Kelly, E.J., Xiao, G., 2018. Emerging kidney models to investigate metabolism, transport, and toxicity of drugs and xenobiotics. *Drug Metab. Dispos.* 46, 1692–1702. <https://doi.org/10.1124/dmd.118.082958>.
- Barbier, O., Jacquillet, G., Tauc, M., Cougnon, M., Poujeol, P., 2005. Effect of heavy metals on, and handling by, the kidney. *Nephron Physiol.* 99, 105–110. <https://doi.org/10.1159/000083981>.
- Barnett, L.M.A., Cummings, B.S., 2018. Nephrotoxicity and renal pathophysiology: a contemporary perspective. *Toxicol. Sci.* 164, 379–390. <https://doi.org/10.1093/toxsci/kfy159>.
- Basile, D.P., Anderson, M.D., Sutton, T.A., 2012. Pathophysiology of acute kidney injury. *Compr. Physiol.* 2, 1303–1353. <https://doi.org/10.1002/cphy.c110041>.
- Basile, D.P., Bonventre, J.V., Mehta, R., Nangaku, M., Unwin, R., Rosner, M.H., et al., 2016. Progression after AKI: understanding maladaptive repair processes to predict and identify therapeutic treatments. *J. Am. Soc. Nephrol.* 27, 687–697. <https://doi.org/10.1681/asn.2015030309>.
- Bengatta, S., Arnould, C., Letavernier, E., Monge, M., de Preneuf, H.M., Werb, Z., et al., 2009. MMP9 and SCF protect from apoptosis in acute kidney injury. *J. Am. Soc. Nephrol.* 20, 787–797. <https://doi.org/10.1681/ASN.2008050515>.
- Blanco, V.E., Hernandez, C.V., Scibona, P., Belloso, W., Musso, C.G., 2019. Acute kidney injury pharmacokinetic changes and its impact on drug prescription. *Healthcare* 7, 10. <https://doi.org/10.3390/healthcare7010010>.
- Bray, N.L., Pimentel, H., Melsted, P., Pachter, L., 2016. Near-optimal probabilistic RNA-seq quantification. *Nat. Biotechnol.* 34, 525. <https://doi.org/10.1038/nbt.3519>.
- Çağlayan, C., Kandemir, F.M., Yildirim, S., Kucukler, S., Eser, G., 2019. Rutin protects mercuric chloride-induced nephrotoxicity via targeting of aquaporin 1 level, oxidative stress, apoptosis and inflammation in rats. *J. Trace Elem. Med. Biol.* 54, 69–78. <https://doi.org/10.1016/j.jtemb.2019.04.007>.
- Chen, C.H., Ke, L.Y., Chan, H.C., Lee, A.S., Lin, K.D., Chu, C.S., et al., 2016. Electronegative low density lipoprotein induces renal apoptosis and fibrosis: STRA6 signaling involved. *J. Lipid Res.* 57, 1435–1446. <https://doi.org/10.1194/jlr.M067215>.
- Chevalier, R.L., 2016. The proximal tubule is the primary target of injury and progression of kidney disease: role of the glomerulotubular junction. *Am. J. Physiol. Renal Physiol.* 311, F145–F161. <https://doi.org/10.1152/ajprenal.00164.2016>.
- Correa-Costa, M., Azevedo, H., Amano, M.T., Goncalves, G.M., Hyane, M.I., Cenedeze, M.A., et al., 2012. Transcriptome analysis of renal ischemia/reperfusion injury and its modulation by ischemic pre-conditioning or hemin treatment. *PLoS One* 7, e49569. <https://doi.org/10.1371/journal.pone.0049569>.
- Elshehy, M., Zahran, F., Omran, M., Nabil, A., 2018. DPPD ameliorates renal fibrosis induced by HgCl₂ in rats. *Biosci. Res.* 15, 2416–2425.
- Fielden, M.R., Eynon, B.P., Natsoulis, G., Jarnagin, K., Banas, D., Kolaja, K.L., 2005. A gene expression signature that predicts the future onset of drug-induced renal tubular toxicity. *Toxicol. Pathol.* 33, 675–683. <https://doi.org/10.1080/>

- 01926230500321213.
- Fowler, B.A., 1993. Mechanisms of kidney cell injury from metals. *Environ. Health Perspect.* 100, 57–63. <https://doi.org/10.1289/ehp.9310057>.
- Frazier, K.S., Seely, J.C., Hard, G.C., Betton, G., Burnett, R., Nakatsuji, S., et al., 2012. Proliferative and nonproliferative lesions of the rat and mouse urinary system. *Toxicol. Pathol.* 40, 14S–86S. <https://doi.org/10.1177/0192623312438736>.
- Ganter, B., Tugendreich, S., Pearson, C.I., Ayanoglu, E., Baumhueter, S., Bostian, K.A., et al., 2005. Development of a large-scale chemogenomics database to improve drug candidate selection and to understand mechanisms of chemical toxicity and action. *J. Biotechnol.* 119, 219–244. <https://doi.org/10.1016/j.jbiotec.2005.03.022>.
- Hamadeh, H.K., Knight, B.L., Haugen, A.C., Sieber, S., Amin, R.P., Bushel, P.R., et al., 2002. Methapyriline toxicity: anchorage of pathologic observations to gene expression alterations. *Toxicol. Pathol.* 30, 470–482. <https://doi.org/10.1080/01926230290105712>.
- Han, W.K., Bailly, V., Abichandani, R., Thadhani, R., Bonventre, J.V., 2002. Kidney Injury Molecule-1 (KIM-1): a novel biomarker for human renal proximal tubule injury. *Kidney Int.* 62, 237–244. <https://doi.org/10.1046/j.1523-1755.2002.00433.x>.
- Harbison, R.D., 1998. *Hamilton & Hardy's Industrial Toxicology*. Mosby, St. Louis.
- Hazelhoff, M.H., Bulacio, R.P., Torres, A.M., 2012. Gender related differences in kidney injury induced by mercury. *Int. J. Mol. Sci.* 13. <https://doi.org/10.3390/ijms130810523>.
- Hussain, S., Rodgers, D.A., Duhart, H.M., Ali, S.F., 1997. Mercuric chloride-induced reactive oxygen species and its effect on antioxidant enzymes in different regions of rat brain. *J. Environ. Sci. Health B* 32, 395–409. <https://doi.org/10.1080/03601239709373094>.
- Igarashi, Y., Nakatsu, N., Yamashita, T., Ono, A., Ohno, Y., Urushidani, T., et al., 2015. Open TG-GATEs: a large-scale toxicogenomics database. *Nucleic Acids Res.* 43, D921–D927. <https://doi.org/10.1093/nar/gku955>.
- Imig, J.D., 2005. Epoxide hydrolase and epoxidegenase metabolites as therapeutic targets for renal diseases. *Am. J. Physiol. Renal Physiol.* 289, F496–F503. <https://doi.org/10.1152/ajprenal.00350.2004>.
- Ippolito, D.L., AbdulHameed, M.D.M., Tawa, G.J., Baer, C.E., Permenter, M.G., McDyre, B.C., et al., 2015. Gene expression patterns associated with histopathology in toxic liver fibrosis. *Toxicol. Sci.* 149, 67–88. <https://doi.org/10.1093/toxsci/kfv214>.
- Joshi, D., Srivastav, S.K., Belemkar, S., Dixit, V.A., 2017. Zingiber officinale and 6-gingerol alleviate liver and kidney dysfunctions and oxidative stress induced by mercuric chloride in male rats: a protective approach. *Biomed. Pharmacother.* 91, 645–655. <https://doi.org/10.1016/j.biopha.2017.04.108>.
- Kanehisa, M., Goto, S., 2000. KEGG: kyoto encyclopedia of genes and genomes. *Nucleic Acids Res.* 28, 27–30. <https://doi.org/10.1093/nar/28.1.27>.
- LaVoie, S.P., Summers, A.O., 2018. Transcriptional responses of *Escherichia coli* during recovery from inorganic or organic mercury exposure. *BMC Genomics* 19, 52. <https://doi.org/10.1186/s12864-017-4413-z>.
- López-Novoa, J.M., Rodríguez-Peña, A.B., Ortiz, A., Martínez-Salgado, C., López Hernández, F.J., 2011. Etiopathology of chronic tubular, glomerular and renovascular nephropathies: clinical implications. *J. Transl. Med.* 9, 13. <https://doi.org/10.1186/1479-5876-9-13>.
- Lund, B.-O., Miller, D.M., Woods, J.S., 1993. Studies on Hg(II)-induced H₂O₂ formation and oxidative stress in vivo and in vitro in rat kidney mitochondria. *Biochem. Pharmacol.* 45, 2017–2024. [https://doi.org/10.1016/0006-2952\(93\)90012-L](https://doi.org/10.1016/0006-2952(93)90012-L).
- McDyre, B.C., AbdulHameed, M.D.M., Permenter, M.G., Dennis, W.E., Baer, C.E., Koontz, J.M., et al., 2018. Comparative proteomic analysis of liver steatosis and fibrosis after oral hepatotoxicant administration in Sprague-Dawley rats. *Toxicol. Pathol.* 46, 202–223. <https://doi.org/10.1177/0192623317747549>.
- Miller, S., Pallan, S., Gangji, A.S., Lukic, D., Clase, C.M., 2013. Mercury-associated nephrotic syndrome: a case report and systematic review of the literature. *Am. J. Kidney Dis.* 62, 135–138. <https://doi.org/10.1053/j.ajkd.2013.02.372>.
- Minowa, Y., Kondo, C., Uehara, T., Morikawa, Y., Okuno, Y., Nakatsu, N., et al., 2012. Toxicogenomic multigene biomarker for predicting the future onset of proximal tubular injury in rats. *Toxicology* 297, 47–56. <https://doi.org/10.1016/j.tox.2012.03.014>.
- Oliveira, V.A., Favero, G., Stacchiotti, A., Giugno, L., Buffoli, B., de Oliveira, C.S., et al., 2017. Acute mercury exposition of virgin, pregnant, and lactating rats: histopathological kidney and liver evaluations. *Environ. Toxicol.* 32, 1500–1512. <https://doi.org/10.1002/tox.22370>.
- Parmentier, C., Couttet, P., Wolf, A., Zaccharias, T., Heyd, B., Bachellier, P., et al., 2017. Evaluation of transcriptomic signature as a valuable tool to study drug-induced cholestasis in primary human hepatocytes. *Arch. Toxicol.* 91, 2879–2893. <https://doi.org/10.1007/s00204-017-1930-0>.
- Perazella, M.A., 2018. Pharmacology behind common drug nephrotoxicities. *Clin. J. Am. Soc. Nephrol.* 13, 1897–1908. <https://doi.org/10.2215/cjn.00150118>.
- Perottoni, J., Rodrigues, O.E.D., Paixão, M.W., Zeni, G., Lobato, L.P., Braga, A.L., et al., 2004. Renal and hepatic ALA-D activity and selected oxidative stress parameters of rats exposed to inorganic mercury and organoselenium compounds. *Food Chem. Toxicol.* 42, 17–28. <https://doi.org/10.1016/j.fct.2003.08.002>.
- Pimentel, H., Bray, N.L., Puente, S., Melsted, P., Pachter, L., 2017. Differential analysis of RNA-seq incorporating quantification uncertainty. *Nat. Methods* 14, 687. <https://doi.org/10.1038/nmeth.4324>.
- Pollard, K., Hultman, P., 1997. Effects of mercury on the immune system. *Met. Ions Biol. Syst.* 34, 421–440.
- Pozzi, A., Zent, R., 2013. Integrins in kidney disease. *J. Am. Soc. Nephrol.* 24, 1034–1039. <https://doi.org/10.1681/ASN.2013010012>.
- Rizvi, M.S., Kashani, K.B., 2019. Biomarkers for early detection of acute kidney injury. *J. Appl. Lab. Med.* 2, 386–399. <https://doi.org/10.1373/jalm.2017.023325>.
- Rojas-Franco, P., Franco-Colin, M., Torres-Manzo, A.P., Blas-Valdivia, V., Thompson-Bonilla, M.D.R., Kandir, S., et al., 2019. Endoplasmic reticulum stress participates in the pathophysiology of mercury-caused acute kidney injury. *Ren. Fail.* 41, 1001–1010. <https://doi.org/10.1080/0886022x.2019.1686019>.
- Sahini, N., Selvaraj, S., Borlak, J., 2014. Whole genome transcript profiling of drug induced steatosis in rats reveals a gene signature predictive of outcome. *PLoS One* 9, e114085. <https://doi.org/10.1371/journal.pone.0114085>.
- Schyman, P., Printz, R.L., Estes, S.K., Boyd, K.L., Shiota, M., Wallqvist, A., 2018. Identification of the toxicity pathways associated with thioacetamide-induced injuries in rat liver and kidney. *Front. Pharmacol.* 9, 1272. <https://doi.org/10.3389/fphar.2018.01272>.
- Schyman, P., Printz, R.L., Estes, S.K., O'Brien, T.P., Shiota, M., Wallqvist, A., 2019. Assessing chemical-induced liver injury in vivo from in vitro gene expression data in the rat: the case of thioacetamide toxicity. *Front. Genet.* 10, 1233. <https://doi.org/10.3389/fgene.2019.01233>.
- Segal, E., Friedman, N., Koller, D., Regev, A., 2004. A module map showing conditional activity of expression modules in cancer. *Nat. Genet.* 36, 1090. <https://doi.org/10.1038/ng1434>.
- Sharfuddin, A.A., Molitoris, B.A., 2011. Pathophysiology of ischemic acute kidney injury. *Nat. Rev. Nephrol.* 7, 189–200. <https://doi.org/10.1038/nrneph.2011.16>.
- Shin, Y.J., Kim, K.A., Kim, E.S., Kim, J.H., Kim, H.S., Ha, M., et al., 2018. Identification of aldo-keto reductase (AKR7A1) and glutathione S-transferase pi (GSTP1) as novel renal damage biomarkers following exposure to mercury. *Hum. Exp. Toxicol.* 37, 1025–1036. <https://doi.org/10.1177/0960327117751234>.
- Shiota, M., 2012. Measurement of glucose homeostasis in vivo: combination of tracers and clamp techniques. In: Joost, H.-G., Al-Hasani, H., Schürmann, A. (Eds.), *Animal Models in Diabetes Research*. Humana Press, Totowa, NJ, pp. 229–253.
- Stacchiotti, A., Borsani, E., Rodella, L., Rezzani, R., Bianchi, R., Lavazza, A., 2003. Dose-dependent mercuric chloride tubular injury in rat kidney. *Ultrastruct. Pathol.* 27, 253–259. <https://doi.org/10.1080/019131203099921>.
- Stacchiotti, A., Lavazza, A., Rezzani, R., Borsani, E., Rodella, L., Bianchi, R., 2004. Mercuric chloride-induced alterations in stress protein distribution in rat kidney. *Histol. Histopathol.* 19, 1209–1218. <https://doi.org/10.14670/hh-19.1209>.
- Sutherland, J.J., Stevens, J.L., Johnson, K., Elango, N., Webster, Y.W., Mills, B.J., et al., 2019. A novel open access web portal for integrating mechanistic and toxicogenomic study results. *Toxicol. Sci.* 170, 296–309. <https://doi.org/10.1093/toxsci/kfz101>.
- Te, J.A., AbdulHameed, M.D.M., Wallqvist, A., 2016. Systems toxicology of chemically induced liver and kidney injuries: histopathology-associated gene co-expression modules. *J. Appl. Toxicol.* 36, 1137–1149. <https://doi.org/10.1002/jat.3278>.
- Thukral, S.K., Nordone, P.J., Hu, R., Sullivan, L., Galambos, E., Fitzpatrick, V.D., et al., 2005. Prediction of nephrotoxicant action and identification of candidate toxicity-related biomarkers. *Toxicol. Pathol.* 33, 343–355. <https://doi.org/10.1080/0192623050927230>.
- Tokumoto, M., Lee, J.Y., Shimada, A., Tohyama, C., Satoh, M., 2018. Glutathione has a more important role than metallothionein-I/II against inorganic mercury-induced acute renal toxicity. *J. Toxicol. Sci.* 43, 275–280. <https://doi.org/10.2131/jts.43.275>.
- Trebucovich, M.S., Hazelhoff, M.H., Chevalier, A.A., Passamonti, S., Brandoni, A., Torres, A.M., 2014. Protein expression of kidney and liver bilitranslocase in rats exposed to mercuric chloride—a potential tissular biomarker of toxicity. *Toxicol. Lett.* 225, 305–310. <https://doi.org/10.1016/j.toxlet.2013.11.022>.
- Waikar, S.S., Betensky, R.A., Bonventre, J.V., 2009. Creatinine as the gold standard for kidney injury biomarker studies? *Nephrol. Dial. Transplant.* 24, 3263–3265. <https://doi.org/10.1093/ndt/gfp428>.
- Waikar, S.S., Betensky, R.A., Emerson, S.C., Bonventre, J.V., 2012. Imperfect gold standards for kidney injury biomarker evaluation. *J. Am. Soc. Nephrol.* 23, 13–21. <https://doi.org/10.1681/asn.2010111124>.
- Wang, H., Liu, R., Schyman, P., Wallqvist, A., 2019. Deep neural network models for predicting chemically induced liver toxicity endpoints from transcriptomic responses. *Front. Pharmacol.* 10, 1–12. <https://doi.org/10.3389/fphar.2019.00042>.
- Wilks, M.F., Gregg, N.J., Bach, P.H., 1994. Metal accumulation and nephron heterogeneity in mercuric chloride-induced acute renal failure. *Toxicol. Pathol.* 22, 282–290. <https://doi.org/10.1177/019262339402200306>.
- Yanagisawa, H., Nodera, M., Kurihara, N., Wada, O., 1998. Altered expression of endothelin-1 and endothelial nitric oxide synthase in the juxtaglomerular apparatus of rats with HgCl₂-induced acute renal failure. *Toxicol. Lett.* 98, 181–188. [https://doi.org/10.1016/S0378-4274\(98\)00122-2](https://doi.org/10.1016/S0378-4274(98)00122-2).
- Zalups, R.K., 2000. Molecular interactions with mercury in the kidney. *Pharmacol. Rev.* 52, 113–144.
- Zerbin, D.R., Achuthan, P., Akanni, W., Amode, M.R., Barrell, D., Bhai, J., et al., 2018. Ensembl 2018. *Nucleic Acids Res.* 46, D754–D761. <https://doi.org/10.1093/nar/gkx1098>.